The FEBS Journal

FEBS PRESS science publishing by scientists

Lipids uniquely alter the secondary structure and toxicity of amyloid beta 1–42 aggregates

Kiryl Zhaliazka[1], Mikhail Matveyenka[1] and Dmitry Kurouski[1,2]

1 Department of Biochemistry and Biophysics, Texas A&M University, College Station, Texas, USA
2 Department of Biomedical Engineering, Texas A&M University, College Station, Texas, USA

Keywords
AFM-IR; amyloid $\beta_{1\text{-}42}$; fibrils; oligomers; phospholipids

Correspondence
D. Kurouski, Department of Biochemistry and Biophysics, Texas A&M University, College Station, Texas 77843, USA
Tel: 979-458-3448
E-mail: dkurouski@tamu.edu

(Received 4 October 2022, revised 25 November 2022, accepted 25 January 2023)

doi:10.1111/febs.16738

Abrupt aggregation of amyloid $\beta_{1\text{-}42}$ (Aβ) peptide is a hallmark of Alzheimer's disease (AD), a severe pathology that affects more than 44 million people worldwide. A growing body of evidence suggests that lipids can uniquely alter rates of $A\beta_{1\text{-}42}$ aggregation. However, it remains unclear whether lipids only alter rates of protein aggregation or also uniquely modify the secondary structure and toxicity of $A\beta_{1\text{-}42}$ oligomers and fibrils. In this study, we investigated the effect of phosphatidylcholine (PC), cardiolipin (CL), and cholesterol (Chol) on $A\beta_{1\text{-}42}$ aggregation. We found that PC, CL and Chol strongly accelerated the rate of fibril formation compared to the rate of $A\beta_{1\text{-}42}$ aggregation in the lipid-free environment. Furthermore, anionic CL enabled the strongest acceleration of $A\beta_{1\text{-}42}$ aggregation compared to zwitterionic PC and uncharged Chol. We also found that PC, CL and Chol uniquely altered the secondary structure of early-, middle- and late-stage $A\beta_{1\text{-}42}$ aggregates. Specifically, CL and Chol drastically increased the amount of parallel β-sheet in $A\beta_{1\text{-}42}$ oligomers and fibrils grown in the presence of these lipids. This caused a significant increase in the toxicity of Aβ : CL and Aβ : Chol compared to the toxicity of Aβ : PC and $A\beta_{1\text{-}42}$ aggregates formed in the lipid-free environment. These results demonstrate that toxicity of Aβ aggregates correlates with the amount of their β-sheet content, which, in turn, is determined by the chemical structure of lipids present at the stage of $A\beta_{1\text{-}42}$ aggregation.

Introduction

Alzheimer's disease (AD) is a severe progressive pathology that is characterized by irreversible deterioration of memory, as well as a substantial impairment of cognition and behaviour [1–3]. There are more than 6 million AD patients in the US alone, whereas the number of people diagnosed with AD in the world is reaching 44 million [4]. AD is characterized by a progressive degradation of neurons in the frontal cortex of the brain [5]. Although the exact cause of the neurodegeneration is unclear, there is a growing body of evidence that AD can be linked to the abrupt aggregation of amyloid $\beta_{1\text{-}42}$ (Aβ). This protein aggregates forming highly toxic oligomers and fibrils [6,7]. Solid-state nuclear magnetic resonance (ss-NMR) and cryo-electron microscopy (cryo-EM) allowed for the elucidation of the secondary structure of Aβ fibrils with Angstrom spatial resolution [8–11]. It was found that Aβ peptide formed two β-sheets with ~ 4.7 Å inter-strand distances that self-assembly forming cross-β-sheet, thermodynamically stable structure that has ~ 10 Å distance between two β-sheets [12–14]. The cross-β-sheet structure stretch microns in length forming filaments which, in turn, can intertwine and coil with other filaments building mature fibrils [15–17].

Abbreviations
AFM-IR, atomic force microscopy Infrared spectroscopy; Aβ, amyloid $\beta_{1\text{-}42}$; Chol, cholesterol; CL, cardiolipin; LDH, lactate dehydrogenase; LUVs, large unilamellar vesicles.; PC, phosphatidylcholine; ThT, thioflavin T.

Aβ oligomers are transient specimens with a large distribution of shapes and sizes [18–20]. Their morphological heterogeneity, as well as low concentrations of Aβ oligomers, limit the use of ss-NMR and cryo-EM for their studies. These limitations can be overcome with several optical nanoscopy techniques such as atomic force microscope Infrared (AFM-IR) spectroscopy [21–26]. In AFM-IR, the metalized scanning probe is positioned on the sample of interest [26–28]. Next, the scanning probe is illuminated by light, which causes thermal expansion in the protein sample [29,30]. These thermal expansions are collected by the scanning probe and then transformed into IR spectra, which, in turn, can be used to determine the protein secondary structure of the analysed specimens [31–33]. Using AFM-IR, Zhou, and co-workers were able to reveal the secondary structure of α-synuclein (α-Syn) oligomers, protein aggregates that are linked to Parkinson's disease [34]. It was found that in the early stages of protein aggregation, two distinctly different types of oligomers were formed. One of them is dominated by α-helical/unordered structure, whereas the second type of oligomers was primarily composed of anti-parallel- and parallel-β-sheet [34]. Furthermore, the oligomers with α-helical/unordered structure remained unchanged during protein aggregation, whereas β-sheet-rich oligomers propagated into fibrils [34]. Similar findings were reported by Hemmingsen and Ghosh groups that investigated structural heterogeneity of $A\beta_{1\text{-}40}$ and Tau aggregates, respectively [35,36]. Using time-resolved IR, Peralvarez-Marin investigated aggregation of a short Aβ fragment ($A\beta_{1\text{-}28}$) [37]. It was found that this peptide first adopted a β-strand before further assembly into fibrils. Several research groups recently demonstrated that Aβ oligomers were dominated by anti-parallel β-sheet secondary structure, as was evident from an intense band at 1695 cm^{-1} in the IR spectra acquired from these aggregates [18,38]. It was also found that IR spectra acquired from mature Aβ fibrils exhibit vibrational bands ~ 1630 cm^{-1}, which correspond to the parallel β-sheet [19,39,40]. Based on these findings researchers proposed that such anti-parallel to parallel β-sheet rearrangement was taken place upon the preparation of oligomers into fibrils [41,42]. Finally, experimental findings reported by Popova *et al.* [43] demonstrated that parallel *vs* anti-parallel β-sheet secondary structure of Aβ fibrils is primarily determined by the length of the peptide. Specifically, it was found that $A\beta_{1\text{-}40}$ formed fibrils with parallel β-sheet, whereas a short $A\beta_{34\text{-}42}$ with anti-parallel β-sheet secondary structure.

A growing body of evidence suggests that lipids can uniquely alter the secondary structure of amyloid oligomers and fibrils [44,45]. Dou and co-workers discovered that phosphatidylcholine (PC) and phosphatidylserine (PS) uniquely altered the secondary structure of α-Syn oligomers present at the early stages of protein aggregation compared to the oligomers formed in the lipid-free environment [46]. Similar findings were recently made by Rizevsky and co-workers [47]. Specifically, the researchers found that cardiolipin (CL) and PC uniquely altered the secondary structure and toxicity of both oligomers and fibrils. Furthermore, utilization of AFM-IR revealed that both PC and PS were present in the structure of α-Syn oligomers [46]. These findings suggested that lipids templated protein aggregation. Several research groups demonstrated that such templation is initiated by electrostatic interactions that are developed between polar heads of lipids and charge amino acids of proteins. Consequently, chemical structure of the lipid can uniquely alter the stability and aggregation properties of amyloidogenic proteins. Zhang *et al.* found that low levels of anionic lipids promoted aggregation of islet amyloid precursor protein (IAPP), as well as facilitated membrane permeability of the corresponding IAPP-lipid aggregates. At the same time, zwitterionic lipid did not alter the rate of IAPP aggregation, whereas cholesterol at or below physiological levels significantly decelerated IAPP amyloid formation and lowered the propensity of IAPP aggregates to cause membrane leakage [48]. Matveyenka *et al.* decently demonstrated that protein-lipid aggregates induce irreversible endoplasmic reticulum (ER) stress in neuronal cells. Since ER and mitochondria are a continuous tubular network of membranes in the cytoplasm, one can expect that amyloid aggregates can also induce ER-associated mitochondrial impairment.

Microscopic examination revealed a significant reduction in the number of mitochondria in pyramidal neurons located in the frontal cortex of AD patients compared to the number of mitochondria present in neurons of healthy individuals [49]. Furthermore, such AD patients exhibit substantial mitochondrial abnormalities and mitochondrial dysfunctions [50,51]. Using Drosophila models, Iijima-Ando *et al.* [52] demonstrated that Aβ induced abnormal mitochondrial dynamics is an early stage of neurodegeneration. Fragmented mitochondria were also observed near amyloid plaques in an APP transgenic model using an *in vivo* multiphoton imaging [53]. All these factors, as well as the reduced levels of critical components of the electron transport chain in the brain of AD patients, suggest that mitochondrial impairment can be the underlying cause of AD [54,55].

Expanding upon this, we investigate the role of mitochondrial lipids in the aggregation properties of

Aβ. Specifically, we aim to determine the extent to which PC, CL and cholesterol (Chol) can alter the rate of Aβ aggregation. PC is a zwitterion that dominates in the mitochondrial membranes of eukaryotic cells, including astrocytes and neurons [56]. CL is a unique negatively charged lipid that occupies around 20% of the inner mitochondrial membrane, whereas it regulates electron transport complexes, carrier proteins and phosphate kinase [57,58]. Mitochondrial membrane also contains around 5% of cholesterol (Chol) that determines the fluidity of the lipid bilayer [59,60]. We also utilize a set of biophysical methods that include AFM-IR, circular dichroism and conventional infrared (IR) spectroscopy to examine the secondary structure of Aβ oligomers and fibrils that were grown in the presence of PC, CL and Chol. Finally, we determine the extent to which these lipids change the toxicity of Aβ aggregates.

Results

Lipids uniquely alter the rate of Aβ aggregation

At pH 7.4, Aβ rapidly aggregates forming oligomers and fibrils, protein aggregates that enhance the fluorescence of thioflavin T (ThT). Therefore, we used ThT fluorescence to investigate the extent to which lipids alter the rate of Aβ aggregation. In the lipid-free environment, Aβ exhibited a short lag phase (t_{lag} = 1.8 ± 0.2 h), which was followed by a rapid increase in the ThT signal that reaches 50% ($t_{1/2}$) of its maximal value at 17 ± 0.2 h and 90% (t_{grow}) at 40 ± 0.2 h, Fig. 1. Our results showed that phosphatidylcholine (PC) drastically shortened t_{lag} = 1.5 ± 0.2 h of Aβ aggregation. Furthermore, PC accelerated Aβ aggregation which was evident from the significantly reduced $t_{1/2}$ = 10.5.0 ± 0.2 h. However, at the late stage, rates of Aβ and Aβ : PC aggregation appeared to be very similar (t_{grow} = 40 ± 0.2 h). Based on these findings, we can conclude that PC promotes the formation of oligomers. However, it has a very small if any effect on the rate of oligomer propagation into fibrils.

In the presence of cardiolipin (CL), Aβ exhibited even shorter t_{lag} = 1.0 ± 0.2 h and smaller values of $t_{1/2}$ = 6.0 ± 0.2 h and t_{grow} = 13 ± 0.2 h. Thus, CL strongly facilitated Aβ aggregation and, unlike PC, enhanced the propagation of oligomers into fibrils. These results are in good agreement with the experimental findings reported by Galvagnion and coworkers. Specifically, the researchers showed that the presence of LUVs of phospholipids allows for a rapid increase in the local concentration of α-Syn on their surfaces, which promotes protein assembly into oligomers and fibrils.

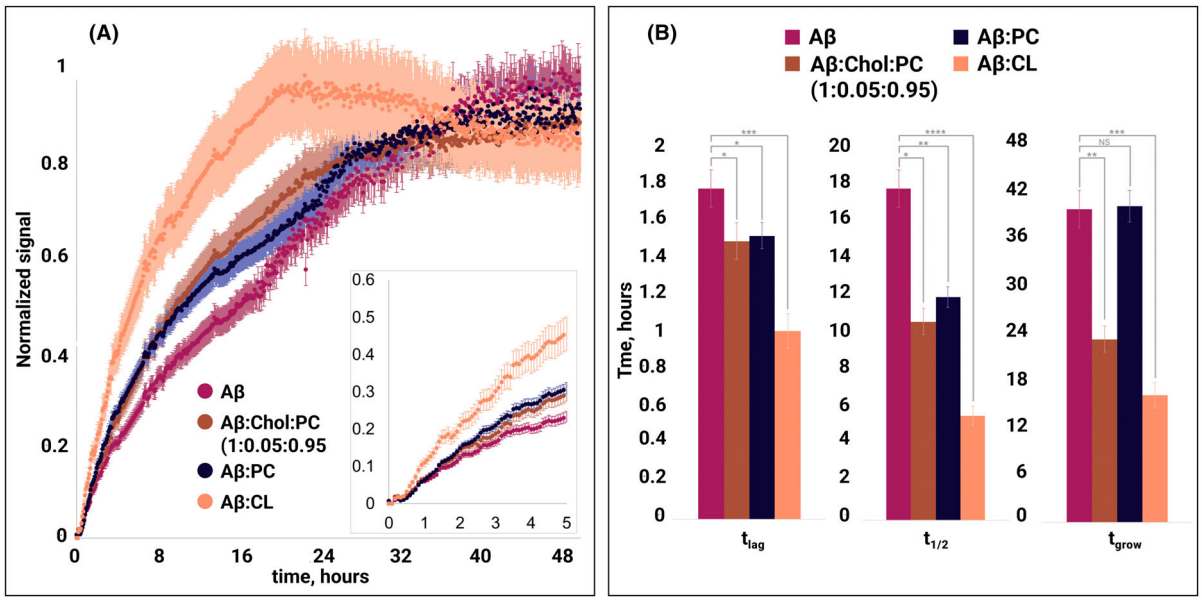

Fig. 1. ThT kinetics (A) of $A\beta_{1\text{-}42}$ (amyloid $\beta_{1\text{-}42}$) aggregation in the presence of LUVs (large unilamellar vesicles) and the lipid-free environment with the histograms (B) of t_{lag}, $t_{1/2}$, and t_{grow}, where statistical analysis was performed using one-way ANOVA, shows significant differences for all testing groups, *n*-value – 10, *P*-value – 0.000232. Two-tailed Student's *t*-test was performed for multiple comparison procedures, and the statistical test error bars represent standard deviation,

Neuronal membranes contain ~ 5% of cholesterol (Chol), a lipid that lowers the fluidity of plasma membranes. Therefore, it becomes important to investigate whether Chol can alter the rate of Aβ aggregation. For this, we exposed monomeric Aβ to the mixture of Chol and PC (5 : 95 mol%). We found that 5% Chol in PC only insignificantly altered the rate of Aβ aggregation relative to the protein aggregation in the presence of PC itself (t_{lag} = 1.5 ± 0.2 h, $t_{1/2}$ = 12.0 ± 0.2 h). However, we found that Aβ : Chol : PC drastically enhanced t_{grow} of the protein aggregation, which was not evident for Aβ : PC. These findings show that Chol does not significantly alter the rate of oligomer formation. However, this lipid strongly facilitates the propagation of oligomers into fibrils.

Elucidation of morphology and protein secondary structure of Aβ oligomers grown in the presence of lipids and in a lipid-free environment

Based on the kinetic results discussed above, we analysed the topology and secondary structure of Aβ aggregates present at the early (3 h), middle (22 h), and late (48 h) stages of protein aggregation. We found that early-stage Aβ aggregates had a spherical appearance with heights ranging from 2 to 5 nm, Fig. 2A,G. Morphologically similar aggregates were observed for Aβ : PC, Aβ : CL and Aβ : Chol : PC. Their height ranged from 2 to 9 nm, Fig. 2G. It should be noted that in addition to the oligomers, Aβ : PC possessed large spherical lipid clusters (200–300 nm in diameter) that were not observed in Aβ : CL and Aβ : Chol : PC, Fig. 3. Next, we performed a systematic AFM-IR analysis of at least 50 individual aggregates observed in Aβ, Aβ : PC, Aβ : CL and Aβ : Chol : PC. The acquired spectra provided information about the secondary structure of these protein specimens. Specifically, we were able to quantify the amount of parallel (1630 cm^{-1}) and anti-parallel (1694 cm^{-1}) β-sheet, as well as unordered protein (1667 cm^{-1}) in the secondary structure of Aβ aggregates [30,46,61,62]. AFM-IR images of protein oligomers revealed relatively similar abundance of these protein secondary structures in the oligomers observed in each of the samples. These findings suggest that such oligomers exhibit low structural diversity. Our results also showed that the protein secondary structure of the early stage Aβ : PC and Aβ oligomers

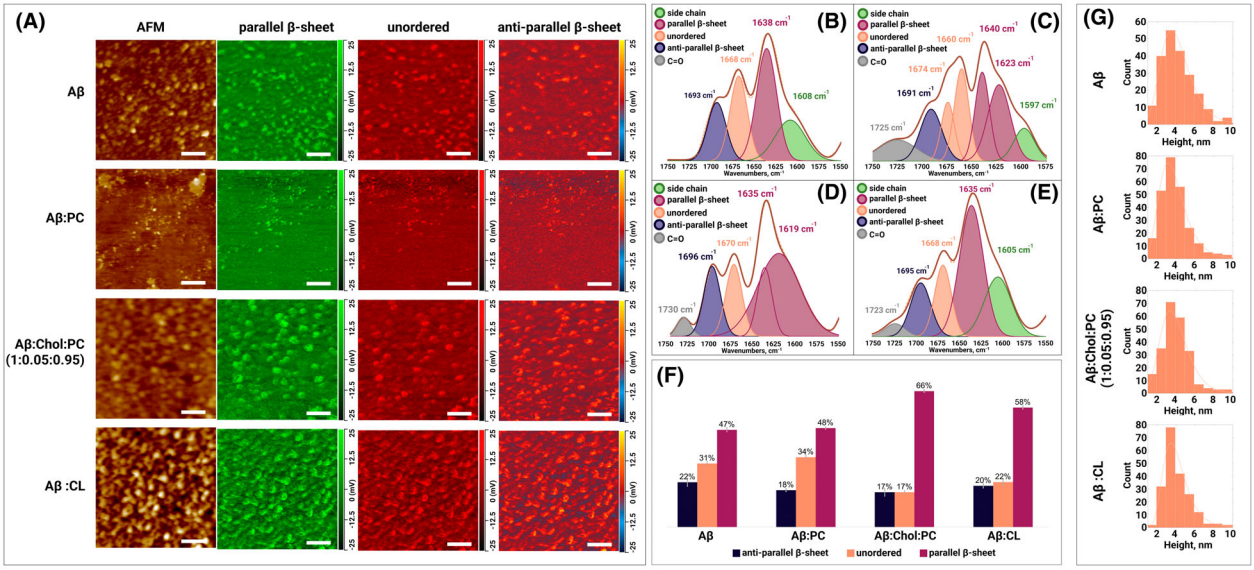

Fig. 2. (A) AFM height images and IR absorption maps of Aβ (amyloid $β_{1-42}$) oligomers formed at the early stage (3 h) of protein aggregation in the absence and presence of PC (phosphatidylcholine), Chol (cholesterol) : PC and CL (cardiolipin). IR absorption maps at 1630 cm^{-1} reveal distribution of parallel β-sheet, at 1667 cm^{-1} unordered protein, and at 1694 cm^{-1} anti-parallel β-sheet. Scale bars are 200 nm. Averaged IR spectra of Aβ (B), Aβ : PC (C), Aβ : Chol : PC (D) and Aβ : CL (E) oligomers with the fitted protein secondary structures. Histogram (F) summarizes relative amount of parallel β-sheet, unordered protein, and anti-parallel β-sheet in the analysed oligomers. Statistical analysis was performed using one-way ANOVA and shows significant differences for all testing groups, *n*-value – 10, *P*-value – 0.000563. Tukey's HSD *post hoc* was performed for multiple comparison procedures and the statistical test showed the following difference between tested groups, error bars represent standard deviation. Corresponding *P*-values listed in supplementary tables. (G) Height profile of short aggregates at the early stage (3 h) of protein aggregation in the absence and presence of PC, Chol : PC and CL.

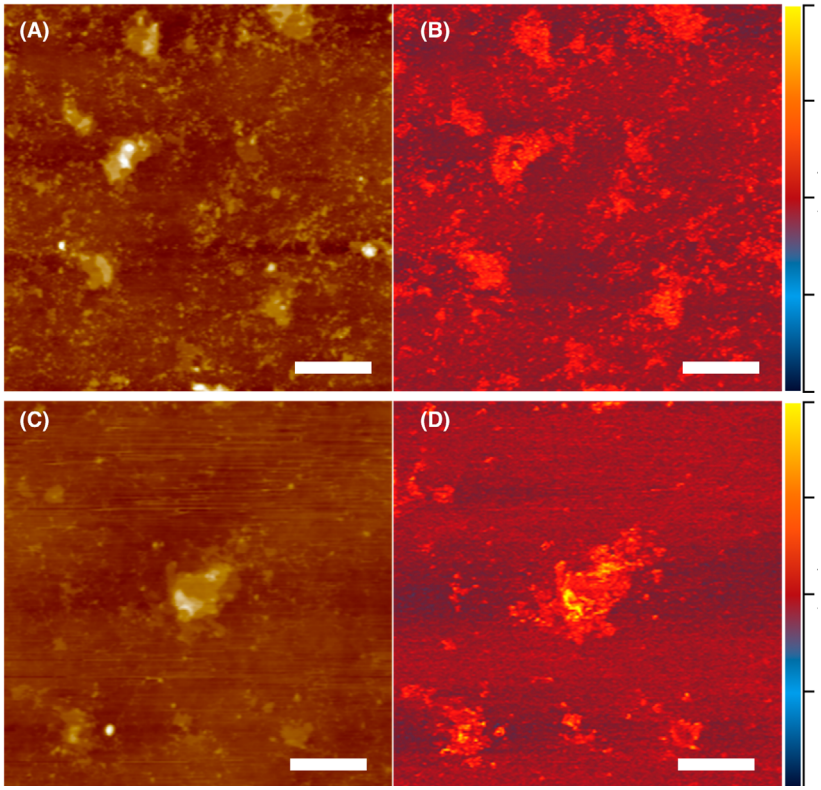

Fig. 3. IR absorption map at 1100 cm − 1 (B, D) and AFM pictures (A, C) of Ab : PC after 3 h of incubation. Scale bars 0.4 μm.

grown in the lipid-free environment was very similar, Fig. 2B–F,G, and Table S1. Specifically, these oligomers contained ~ 47% parallel and ~ 20% anti-parallel β-sheet with ~ 32% of unordered protein secondary structure. However, both Aβ : CL and Aβ : Chol : PC oligomers exhibited significantly higher content of parallel β-sheet and significantly lower amount of unordered protein in their secondary structure. It should be noted that all analysed early-stage oligomers had very similar amount (17–22%) of anti-parallel β-sheet in their secondary structure. Thus, we can conclude that lipids uniquely altered the secondary structure of Aβ oligomers formed at the early stages of protein aggregation.

Middle stage Aβ oligomers exhibited spherical appearance with an average height of ~ 4 nm. Morphologically similar oligomers were observed for Aβ : CPC, Aβ : CL and Aβ : Chol : PC, Fig. 4A. AFM-IR analysis of protein oligomers observed at the middle stage of Aβ aggregation revealed an increase in the amount of parallel β-sheet in Aβ : PC relative to Aβ themselves, Fig. 4B–F and Table S1. Furthermore, Aβ : CL and Aβ : Chol : PC oligomers possessed a greater amount of parallel β-sheet than Aβ : PC aggregates. We observed the opposite distribution of anti-parallel β-sheet in these protein species. Specifically, Aβ : Chol : PC oligomers exhibited the lowest (9%), whereas Aβ had the highest (26%) amount of anti-parallel β-sheet, Fig. 4B–F and Table S1. Finally, all middle stages of Aβ aggregates possessed similar amount of unordered protein in their secondary structure.

We observed drastic differences in the secondary structure of late-stage (48 h) Aβ oligomers grown in the lipid-free environment, as well as in the presence of PC, CL and Chol : PC, Fig. 5. Specifically, Aβ and Aβ : CL oligomers exhibited ~ 61% of parallel β-sheet in their secondary structure. Aβ : PC oligomers possessed significantly lower (50%), whereas Aβ : Chol : PC oligomers had significantly higher (69%) amount of parallel β-sheet in their secondary structure compared to both Aβ and Aβ : CL oligomers. At the same time, the amount of anti-parallel β-sheet was very similar in Aβ and Aβ : Chol : PC (~ 10%) oligomers, Table S1. Finally, these late-stage protein species exhibited drastically different content of unordered protein. Specifically, we found that Aβ : PC oligomers contained ~ 33%, whereas Aβ : Chol : PC ~ 22% of unordered protein in their secondary structure. At the same time, the amount of this secondary structure was found to be very similar in Aβ and Aβ : CL (~ 27%) oligomers, Table S1. Thus, we can conclude that lipids uniquely alter the secondary structure of Aβ aggregates present on the late stage of

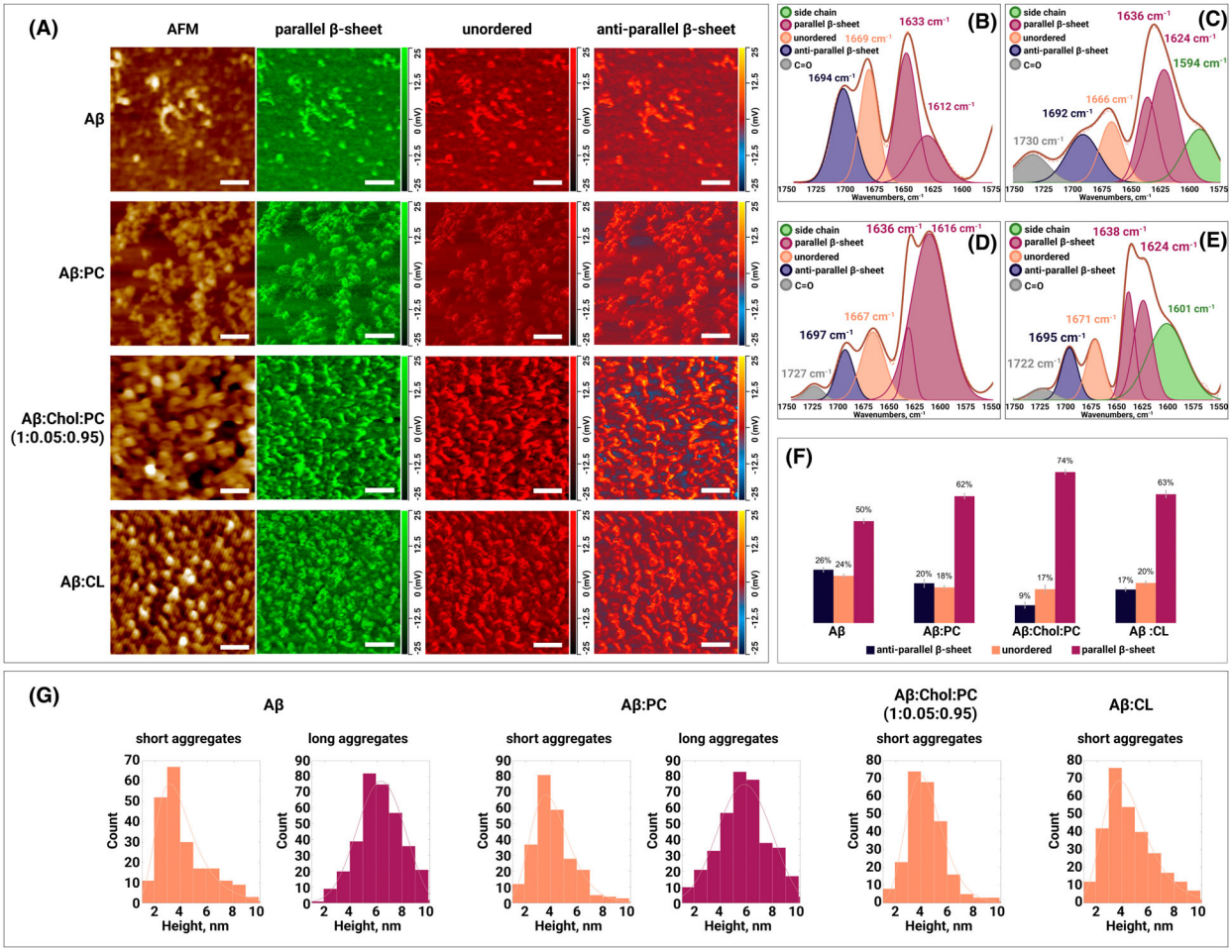

Fig. 4. (A) AFM height images and IR absorption maps of Aβ (amyloid β_{1-42}) oligomers formed at the middle stage (22 h) of protein aggregation in the absence and presence of PC (phosphatidylcholine), Chol (cholesterol) : PC and CL (cardiolipin). IR absorption maps at 1630 cm^{-1} reveal distribution of parallel β-sheet, at 1667 cm^{-1} unordered protein, and at 1694 cm^{-1} anti-parallel β-sheet. Scale bars are 200 nm. Averaged IR spectra of Aβ (B), Aβ : PC (C), Aβ : Chol : PC (D) and Aβ : CL (E) oligomers with the fitted protein secondary structures. Histogram (F) summarizes relative amount of parallel β-sheet, unordered protein and anti-parallel β-sheet in the analysed oligomers. Statistical analysis was performed using one-way ANOVA and shows significant differences for all testing groups, *n*-value – 10, *P*-value – 0.000497. Tukey's HSD *post hoc* was performed for multiple comparison procedures and the statistical test showed the following difference between tested groups; error bars represent standard deviation. Corresponding *P*-values listed in supplementary tables. (G) Height profile of short and long aggregates at the early stage (22 h) of protein aggregation in the absence and presence of PC, Chol : PC and CL.

protein aggregation. It should be noted that a height of all observed inhibiters at this stage ranged from 2 to 9 nm. This indicates that lipids uniquely alter the secondary structure and not morphology of Aβ oligomers formed at the late stage of protein aggregation.

Morphological analysis of protein oligomers formed after 5 days (120 h) of incubation of Aβ in the presence of lipids and in a lipid-free environment revealed presence of both oligomers and fibrils with a height of 3–5 nm and 7–9 nm, respectively (Fig. 6A,B,G). Thus, we can conclude that presence of lipids during Aβ aggregation did not significantly alter the morphologies of Aβ oligomers and fibrils. AFM-IR revealed major changes in the secondary structure of Aβ and Aβ : PC oligomers present at day 5 protein aggregation. Specifically, Aβ : Chol : PC oligomers had a significantly lower amount of parallel β-sheet (32%) than Aβ (55%) and Aβ : CL (60%) oligomers, Fig. 6. Aβ : PC oligomers also possessed nearly twice lower amount of anti-parallel β-sheet (10%) than Aβ (21%) and Aβ : CL (19%) oligomers, Table S1. However, the amount of unordered protein secondary structure was higher in Aβ : PC (43%) oligomers than in Aβ (24%) oligomers. Based on this observation, we can conclude that lipids

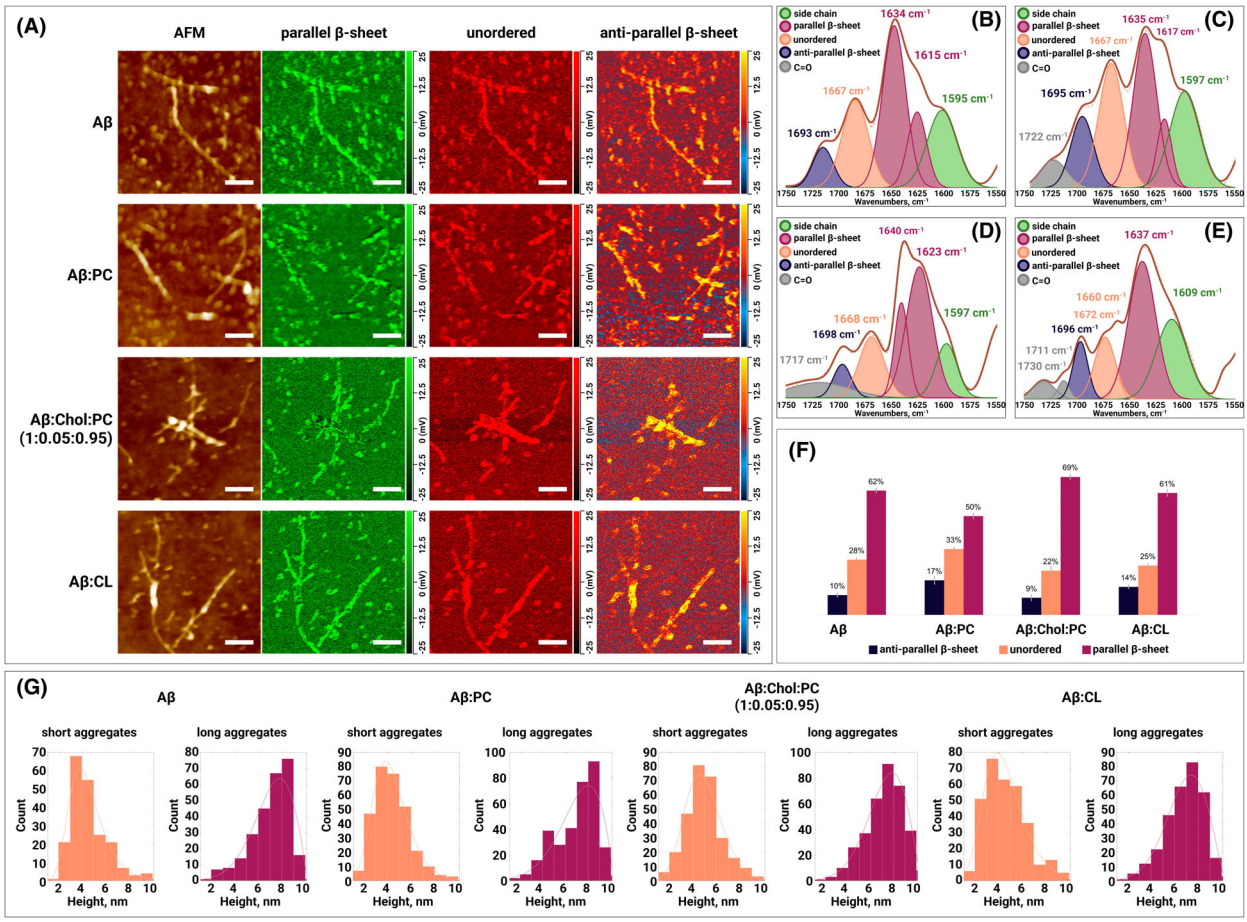

Fig. 5. (A) AFM height images and IR absorption maps of Aβ (amyloid $\beta_{1\text{-}42}$) formed at the late stage (48 h) of protein aggregation in the absence and presence of PC (phosphatidylcholine), Chol (cholesterol) : PC and CL (cardiolipin). IR absorption maps at 1630 cm^{-1} reveal distribution of parallel β-sheet, at 1667 cm^{-1} unordered protein, and at 1694 cm^{-1} anti-parallel β-sheet. Scale bars are 200 nm. Averaged IR spectra of Aβ (B), Aβ : PC (C), Aβ : Chol : PC (D) and Aβ : CL (E) oligomers with the fitted protein secondary structures. Histogram (F) summarizes relative amount of parallel β-sheet, unordered protein and anti-parallel β-sheet in the analysed oligomers. Statistical analysis was performed using One-way ANOVA and shows significant differences for all testing groups, *n*-value – 10, *P*-value – 0.000942. Tukey's HSD *post hoc* was performed for multiple comparison procedures, and the statistical test showed the following difference between tested groups, error bars represent standard deviation. Corresponding *P*-values listed in supplementary tables. (G) Height profile of short and long aggregates at the early stage (48 h) of protein aggregation in the absence and presence of PC, Chol : PC and CL.

drastically altered protein secondary structure of Aβ oligomeric species present at day 5 of protein aggregation.

It should be noted that AFM-IR spectra collected from all oligomers that were grown in the presence of lipids had a well-defined peak around 1720 cm^{-1} (Figs 3–8), which can be assigned to the ester (C=O) vibration of lipids. These findings demonstrate that corresponding lipid molecules are present in Aβ : CL, Aβ : PC and Aβ : Chol : PC oligomers. AFM-IR spectra collected from some of the analysed oligomers also had a shoulder around 1590 cm^{-1} (Figs 2–5), which can be assigned to amino acid side chains of valine and glycine.

Nanoscale structural analysis of Aβ fibrils present at different stages of protein aggregation

At the early (3 h) stage of protein aggregation, we observed no fibrils present in any of the analysed samples. However, at the middle stage (22 h), fibril-like protein species were observed for Aβ and Aβ : PC. We found that Aβ : PC fibrils exhibited a significantly higher amount of parallel β-sheet (75%) than Aβ fibrils (57%), Fig. 7A–C. Aβ : PC fibrils also possessed nearly twice the lower amount of anti-parallel β-sheet and unordered protein secondary structure (15% and 9%, respectively) than Aβ fibrils (22% and 20%,

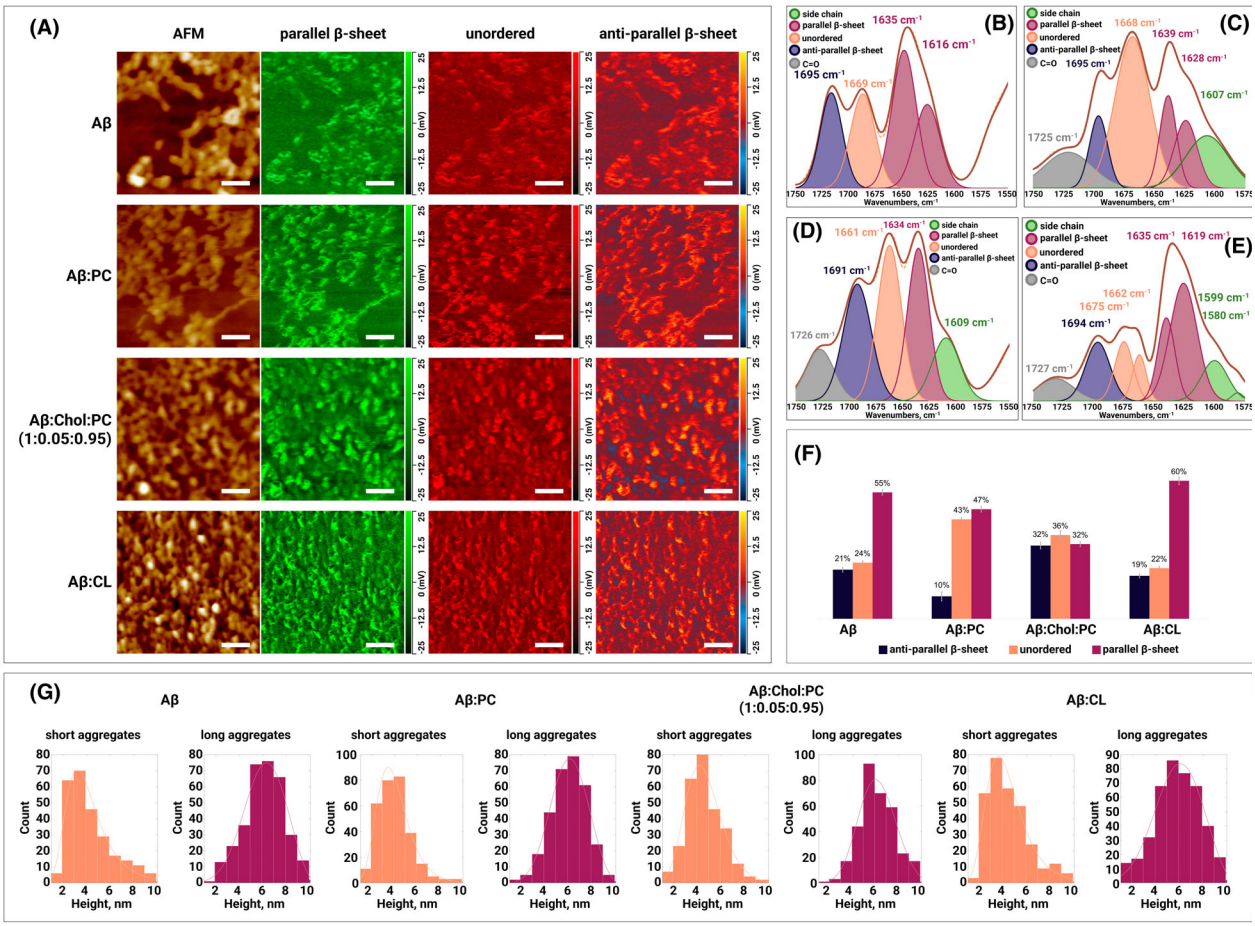

Fig. 6. (A) AFM height images and IR absorption maps of Aβ (amyloid β_{1-42}) oligomers formed at the late stage (day 5) of protein aggregation in the absence and presence of PC (phosphatidylcholine), Chol (cholesterol) : PC and CL (cardiolipin). IR absorption maps at 1630 cm^{-1} reveal distribution of parallel β-sheet, at 1667 cm^{-1} unordered protein, and at 1694 cm^{-1} anti-parallel β-sheet. Scale bars are 200 nm. Averaged IR spectra of Aβ (B), Aβ : PC (C), Aβ : Chol : PC (D) and Aβ : CL (E) oligomers with the fitted protein secondary structures. Histogram (F) summarizes relative amount of parallel β-sheet, unordered protein and anti-parallel β-sheet in the analysed oligomers. Statistical analysis was performed using one-way ANOVA and shows significant differences for all testing groups, *n*-value – 10, *P*-value – 0.000198. Tukey's HSD *post hoc* was performed for multiple comparison procedures, and the statistical test showed the following difference between tested groups; error bars represent standard deviation. Corresponding *P*-values listed in supplementary tables. (G) Height profile of short and long aggregates at the early stage (day 5) of protein aggregation in the absence and presence of PC, Chol : PC and CL.

respectively). AFM-IR analysis of Aβ fibrils that were present at the late state (48 h) in all analysed samples revealed drastic differences in their secondary structure, Fig. 7D–H and Table S2. Specifically, we found that Aβ : PC fibrils exhibited the lowest amount of parallel β-sheet (36%) and the largest amount of unordered protein secondary structure (52%). The amount of parallel β-sheet was found to be different in Aβ : Chol : PC (43%) and Aβ : CL (65%) fibrils compared to the Aβ fibrils formed in the lipid-free environment (53%). Furthermore, Aβ : Chol : PC and Aβ fibrils had nearly twice and three times higher amount of anti-parallel β-sheet than both Aβ : PC and Aβ : CL fibrils, respectively. Thus, we can conclude that the secondary structure of Aβ fibrils directly depends on the lipid present in the protein solution upon their formation. We can also conclude that presence of PC favoured the accumulation of unordered protein secondary structure in Aβ fibrils, whereas the presence of CL yielded fibrils with the highest content of parallel β-sheet. Thus, we can conclude that lipids determine differences in the secondary structure of mature Aβ fibrils. It should be noted that this information about the structure of Aβ fibrils could not be obtained using conventional optical spectroscopy, such as CD or FTIR, Fig. 8A,B.

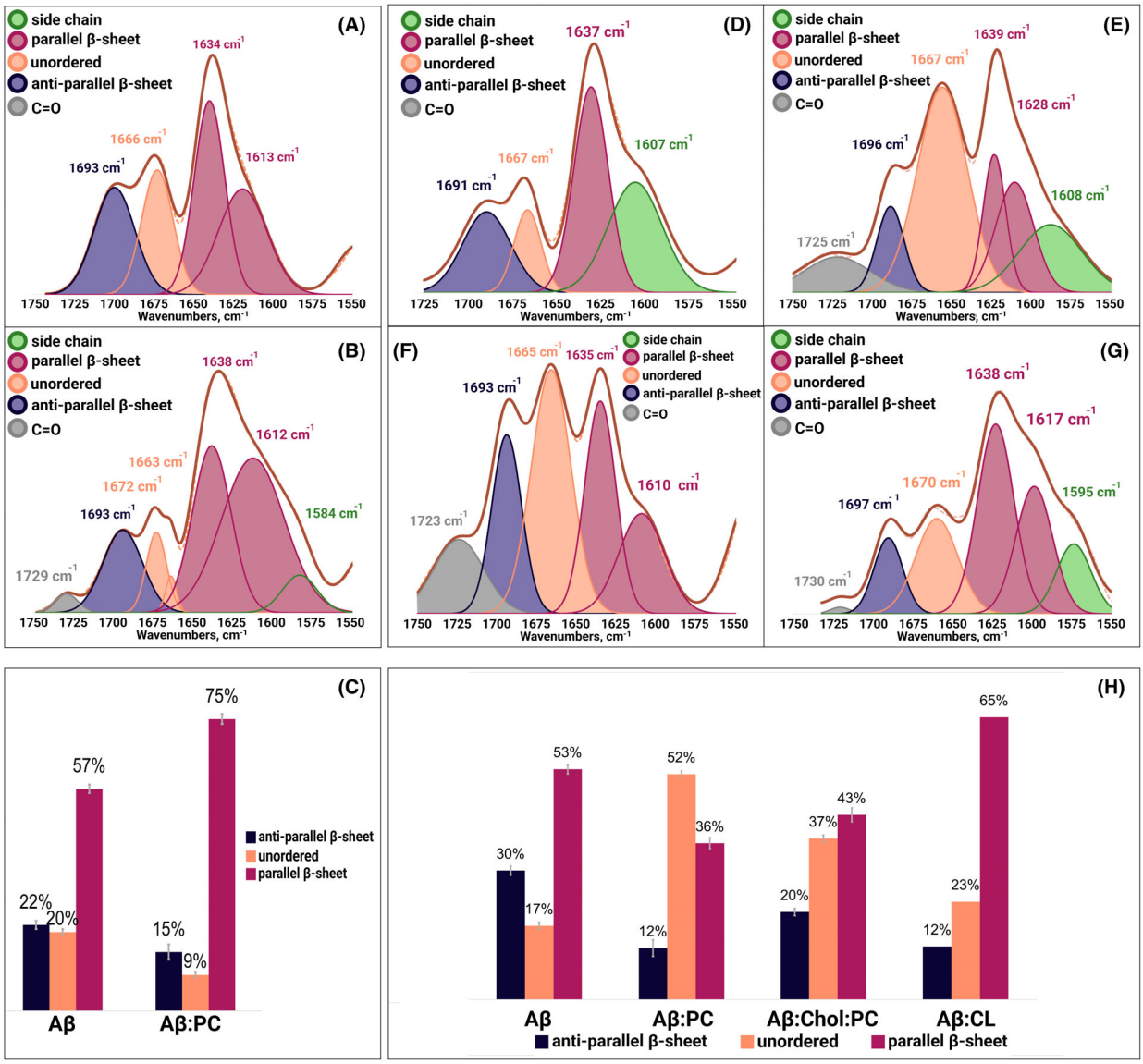

Fig. 7. Averaged IR spectra of Aβ (amyloid $\beta_{1\text{-}42}$) (A) and Aβ : PC (phosphatidylcholine) (B) fibrils formed at 22 h with the fitted protein secondary structures. Histogram (C) summarizes relative amount of parallel β-sheet, unordered protein and anti-parallel β-sheet in the analysed Aβ and Aβ : PC fibrils. Averaged IR spectra of Aβ (D), Aβ : PC (E), Aβ : Chol (cholesterol) : PC (F) and Aβ : CL (cardiolipin) (G) fibrils formed at 48 h with the fitted protein secondary structures. Histogram (H) summarizes relative amount of parallel β-sheet, unordered protein and anti-parallel β-sheet in the analysed Aβ, Aβ : PC, Aβ : Chol : PC and Aβ : CL fibrils. Statistical analysis was performed using one-way ANOVA and shows significant differences for all testing groups, *n*-value – 10, *P*-value – 0.000874. Tukey's HSD *post hoc* was performed for multiple comparison procedures, and the statistical test showed the following difference between tested groups; error bars represent standard deviation. Corresponding *P*-values listed in supplementary tables.

Elucidation of the relationship between protein secondary structure and toxicity of Aβ oligomers and fibrils

One may wonder about the biological significance of the discussed above results. To answer this question, we investigated the extent to which lipids could alter the toxicity of Aβ aggregates using mice midbrain N27 cells. We found that the toxicity of Aβ aggregates that were grown in the presence of lipids at the early, middle, and late stages were greater than the toxicity of Aβ aggregates formed in the lipid-free environment, Fig. 9A and Table S3. Furthermore, the toxicity of Aβ : Chol : PC oligomers was greater than the toxicity of Aβ : CL oligomers. LDH results also showed that

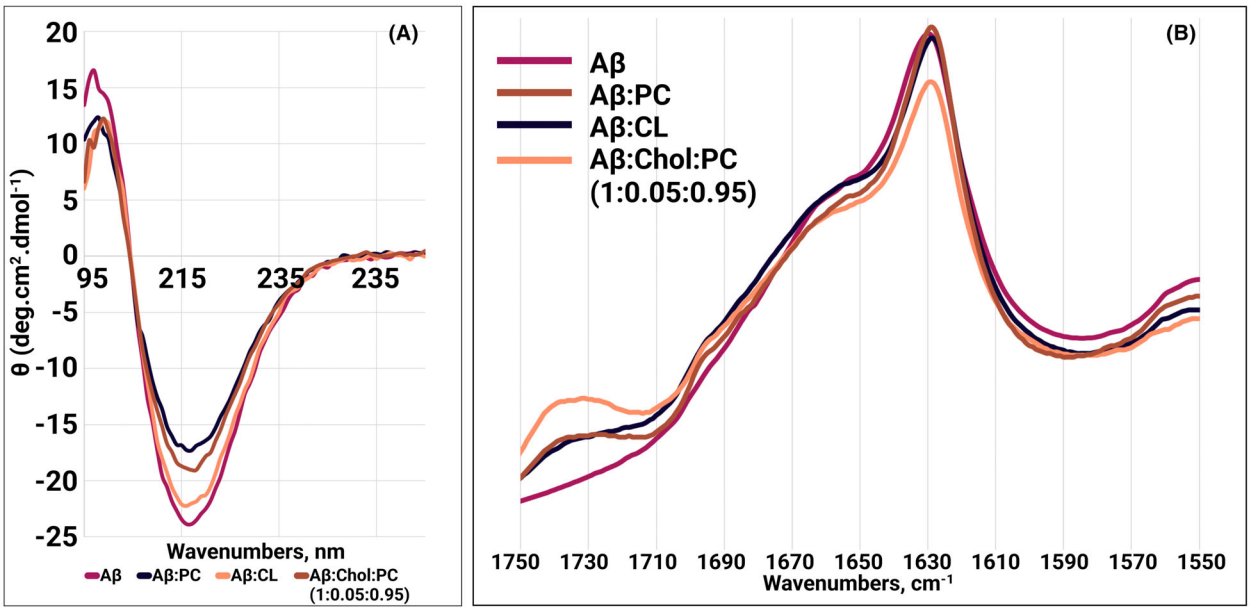

Fig. 8. CD (A) and FTIR (B) spectra of Aβ (amyloid $\beta_{1\text{-}42}$) collected at 5-day time point of protein aggregation in presence of PC (phosphatidylcholine), Chol (cholesterol) : PC and CL (cardiolipin) (0.05 : 0.95) LUVs (large unilamellar vesicles).

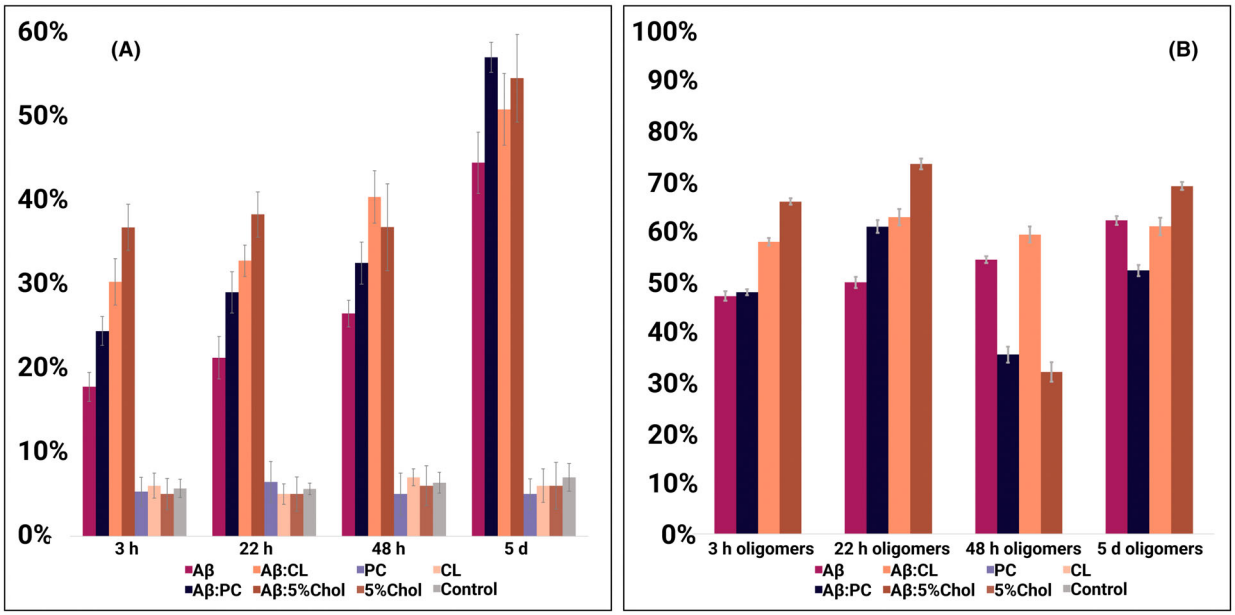

Fig. 9. (A) Results of LDH (lactate dehydrogenase) toxicity assay showing relative toxicity of Aβ (amyloid $\beta_{1\text{-}42}$) aggregates formed at different stages of protein aggregation; (B) Content of parallel β-sheet (1610–1640 cm^{-1}) in an average of short Aβ oligomers by all-time points. Statistical analysis was performed using one-way ANOVA and shows significant differences for all testing groups, *n*-value – 10, *P*-value – 0.000435. Tukey's HSD *post hoc* was performed for multiple comparison procedures, and the statistical test showed the following difference between tested groups; error bars represent standard deviation. Corresponding *P*-values listed in supplementary tables.

the toxicity of Aβ : PC was lower than the toxicity of Aβ : CL and higher than the toxicity of Aβ oligomers grown in the lipid-free environment. These findings show that lipids uniquely alter the toxicity of Aβ oligomers formed at the early stage of protein aggregation.

We also found distinct differences in the toxicity that middle-stage oligomers grown in the presence of lipids and a lipid-free environment. Specifically, Aβ : Chol : PC oligomers exerted the greatest toxicity compared to all analysed protein specimens, Table S3. We also found that the toxicity gradually decreased from Aβ : CL to Aβ : PC and Aβ oligomers. We also found that late-stage Aβ : Chol : PC and Aβ : CL aggregates exerted similar toxicity, which in turn was greater than the toxicity of Aβ : PC and Aβ aggregates, Table S3. Finally, we found that the toxicity of Aβ : Chol : PC, Aβ : CL, Aβ : PC and Aβ fibrils was very similar.

Next, we compared the relative amount of different protein secondary structures in the analysed protein oligomers observed at early, middle and late stages of protein aggregation, Fig. 9B and Table S4. We found a direct correlation between the amount of parallel β-sheet in protein aggregates and the levels of toxicity that was exerted by these samples. Specifically, early-stage Aβ : Chol : PC aggregates possessed the highest amount of parallel β-sheet (~ 68%) compared to all other samples. As was discussed above, these aggregates were the most toxic to the mice's midbrain N27 cells. Aβ : CL contained around 60% of parallel β-sheet and their toxicity was lower compared to the toxicity of Aβ : Chol : PC oligomers. It should be noted that the amount of parallel β-sheet in Aβ and Aβ : PC was very similar (~ 48%), Fig. 9B and Table S4. Consequently, their toxicities were lower than the toxicity of Aβ : Chol : PC and Aβ : CL oligomers. A similar relationship between the amount of parallel β-sheet and toxicity is observed for middle-state Aβ oligomers. These results demonstrate that the toxicity of Aβ oligomers is determined by the amount of parallel β-sheet in their structure, which, in turn, depends on the chemical nature of the lipid present during protein aggregation.

However, we did not observe a direct correlation between the amount of parallel β-sheet and toxicity of oligomers and fibrils formed at the late stages (48 h and day 5). We infer that such relationship was not evident because at those stages both oligomers and fibrils were present. Highly likely, formed oligomers and fibrils exerted drastically different cell toxicities. Therefore, in those samples, no clear relationship between the protein secondary structure and cell toxicity of the aggregates can be observed.

Discussion

A growing body of evidence shows that Aβ has a strong affinity to lipids [63–67]. When exposed to lipid bilayers, the C-terminal hydrophobic region of Aβ adopts an α-helical conformation that facilitates partial insertion of the peptide into membranes [68,69]. These conformational changes trigger Aβ aggregation into oligomers that form Ca^{2+} permeable pores in the lipid bilayers [70,71]. Our findings show that the secondary structure of such Aβ oligomers is determined by the chemical nature of lipid present in the bilayer. Specifically, in the presence of CL, Aβ formed oligomers that possessed a significantly higher amount of parallel β-sheet than the oligomers grown in the presence of PC. Thus, we can conclude that anionic lipids enhance the β-sheet content of early-stage oligomers. Furthermore, the presence of Chol, even at a low molar ratio (5%) in PC, yields Aβ oligomers with the highest (66%) β-sheet content compared to Aβ : CL (58% β-sheet), Aβ : PC (48% β-sheet) and Aβ alone (48% β-sheet), Fig. 9. Based on these results, we can conclude that Chol drastically alters the secondary structure of early-stage Aβ oligomers increasing their β-sheet content. It is important to emphasize that the amount of parallel β-sheet has a direct correlation with the toxicity of Aβ aggregates formed at the early and middle stages of protein aggregation. Therefore, one can expect that lipids modulate the toxicity of Aβ aggregates by altering their β-sheet content. It should be noted that a direct relationship between toxicity and the amount of parallel β-sheet was not evident for Aβ aggregates formed at the late stages [48 h and 120 h (5 days)] of protein aggregation. As was discussed above, at these stages of protein aggregation, in addition to the oligomers AFM imaging revealed presence of fibrils. Previously reported results by our and other research groups demonstrated that Aβ oligomers and fibrils exerted drastically different cell toxicities [72–74]. Thus, two factors determine toxicity of protein aggregates formed at 48 h and 5 days: (a) oligomer *vs* fibril ratio and (b) the amount of parallel β-sheet. Therefore, no direct relationship could be observed between toxicity and the amount of parallel β-sheet for such heterogeneous, from perspective of protein aggregates, samples.

Our results also show that in addition to the structural changes induced in early-stage oligomers, lipids uniquely alter the aggregation rates of Aβ. Specifically, we found that CL strongly accelerates protein aggregation compared to the effects exerted by PC and Chol : PC. These findings are in good agreement with the results reported by Chauhan and co-workers [75]. Specifically, the researchers found that anionic phospholipids accelerated the rate of Aβ aggregation more strongly than zwitterionic lipids. Matveyenka *et al.* [61] previously investigated the effect of PC and CL

on the rate of insulin aggregation. It was found that CL accelerated protein aggregation, whereas PC strongly inhibited insulin fibril formation. At the same time, our ThT results show that PC cause no inhibition of Aβ. Instead, these zwitterionic lipids accelerated Aβ aggregation. This difference could be attributed to the differences in the conformational changes induced by PC on insulin and Aβ. Highly likely, PC stabilizes monomeric insulin [61], which drastically lowers its aggregation properties, whereas conformational changes induced by PC in Aβ, on the opposite, favour its oligomerization and fibril formation. The observed difference in the effect of PC on insulin and Aβ aggregation is also evident for insulin and Aβ oligomers and fibrils. Specifically, PC drastically reduced the toxicity of insulin oligomers, whereas Aβ oligomers that were grown in the presence of PC exerted higher toxicity than Aβ oligomers formed in the lipid-free environment. AFM-IR analysis of insulin oligomers revealed the dominance of unordered proteins in their secondary structure. At the same time, nearly half of Aβ : PC oligomers are occupied by parallel β-sheet. These results further support the direct relationship between the amount of parallel β-sheet and the toxicity of amyloid aggregates. Finally, experimental results reported in this work show that lipids are present in the Aβ aggregates that were formed in the presence of CL, PC and Chol : PC. One can expect that presence of lipids in the structure of oligomers and fibrils can drastically alter their hydrophobicity making them more permeable for lipid bilayers. Thus, the presence of lipids in the Aβ aggregates can be

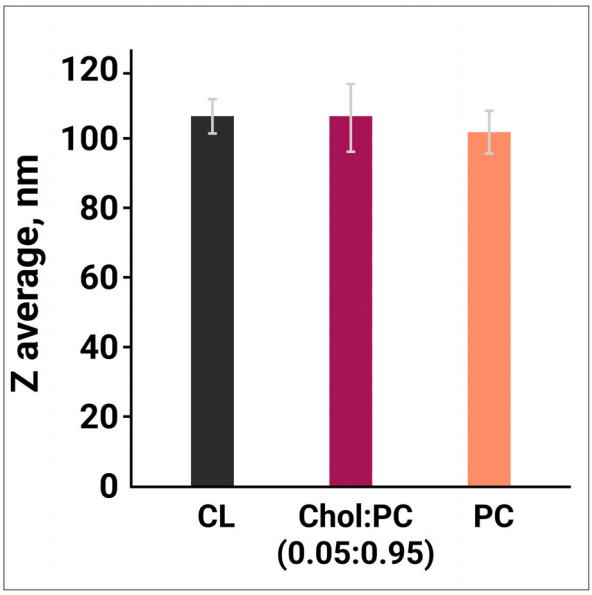

Fig. 10. LUVs (large unilamellar vesicles) radii determined using DLS. Error bars represent standard deviation, *n*-value – 10.

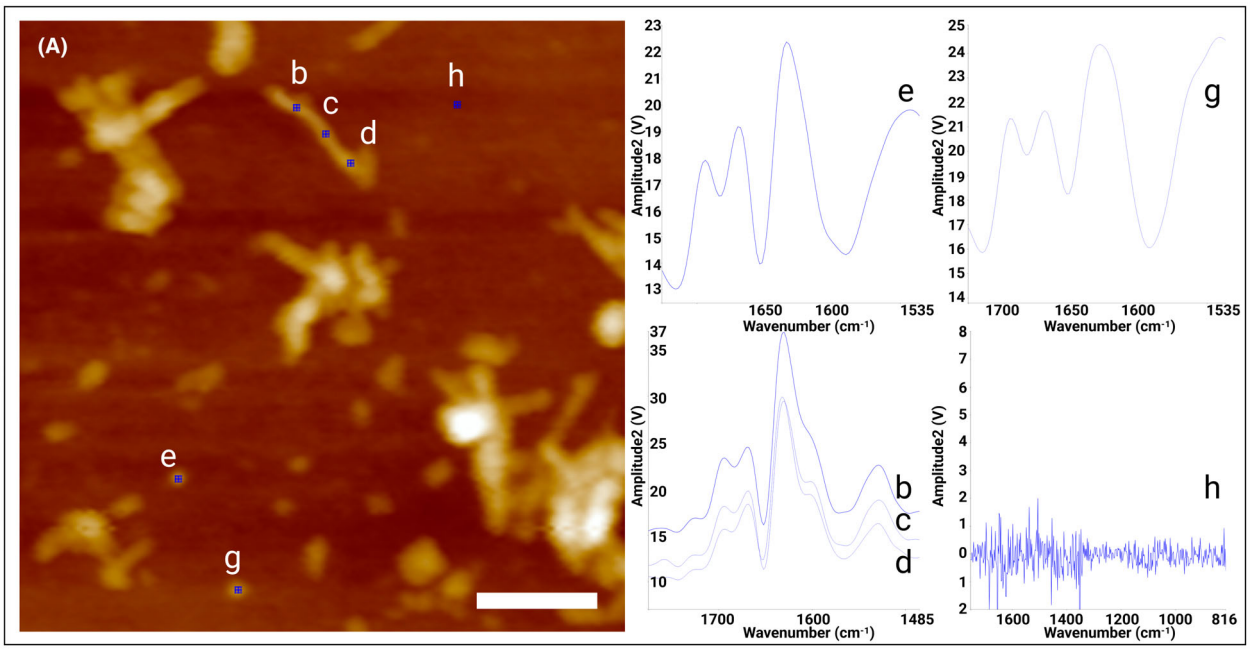

Fig. 11. AFM picture of single Aβ (amyloid $\beta_{1\text{-}42}$) aggregates at 48 h time points (A) and single spectra of short (e, g), long (b–d) Ab42 aggregates and background spectra (h).

caused the increase in their toxicity compared to the lipid-free Aβ oligomers and fibrils.

These results are in a good agreement with the findings of Matveyenka *et al.* [61,76–80] which demonstrated that toxicity of insulin and lysozyme aggregates could be uniquely altered by lipids. Specifically, it was found that presence of PC at 1 : 1 molar ratios with insulin and lysozyme resulted in formation of small oligomers that exerted nearly three times lower cell toxicity compared to proteins fibrils grown in the lipid-free environment [76–78]. Furthermore, these studies demonstrate that lipids also altered rates of insulin and lysozyme aggregation [76–78]. Matveyenka *et al.* [78] recently demonstrated that such protein : lipid oligomers and fibrils were endocytosed by cells. Next, these aggregates damage endosomal membranes leaking into the cytosol. In parallel, protein : lipid oligomers and fibrils activate unfolded protein response, which indicates substantial damage of endoplasmic reticulum (ER), an important cell organelle used for calcium storage, protein synthesis and folding [77]. This leads to the subsequent damage of cell mitochondria and overall enhancement of ROS levels in the cell [76–80].

Conclusions

Our experimental results show that PC, CL and Chol alter the rate of Aβ aggregation. Anionic CL showed the strongest acceleration of Aβ aggregation compared to zwitterionic PC and uncharged Chol. We also found that PC, CL and Chol uniquely altered the secondary structure of oligomers observed at the early-, middle- and late-stage Aβ aggregation. Specifically, CL and Chol drastically increased the amount of parallel β-sheet in Aβ oligomers. This caused an increase in toxicity of these protein species compared to the toxicity of Aβ oligomers grown in the presence of PC. Thus, we can conclude lipids modulate the toxicity of Aβ oligomers by altering their β-sheet content.

Materials and methods

Large unilamellar vesicles (LUVs) preparation

14 : 0 DMPC (PC) (Cat.N. 850345), 18 : 00 cardiolipin (CL) (Cat.N. 710334) and cholesterol (Chol) (Cat.N. 700100) were purchased at Avanti Polar Lipids (Alabaster, AL, USA). PC and CL were dissolved in 20 mM phosphate buffer, pH 7.4 to reach the final concentration of 400 μM. For 5 mol% cholesterol and 95 mol% of PC (Chol : PC), both PC and Chol were first mixed in chloroform at the corresponding molar ratio. After chloroform was evaporated by the N_2 stream, a lipid film was dissolved in 20 mM phosphate buffer, pH 7.4. All lipid samples were exposed to 5 freeze–thaw cycles in liquid nitrogen and a water bath to make LUVs. Finally, lipid solutions were passed through the extruded (Avanti Polar Lipids, Cat.N. 610000) equipped with a 100 nm membrane (Avanti Polar Lipids, Cat.N. 610005) to reach LUVs with ~ 100 nm dimeter, Fig. 10.

Dynamic light scattering (DLS)

LUV diameter was determined by DLS using a Zetasizer Nano S. For each measurement, a solution of lipids was placed in a quartz cuvette with a 3 mm path length.

Protein aggregation

1 mg of recombinant human $A\beta_{1\text{-}42}$ (Gene Script Cat.No RP10017; Piscataway, NJ, USA) was dissolved in 1 mL of HFIP (Across Organics, code 445820500; Waltham, MA, USA); after all, peptide was fully dissolved, HFIP was evaporated under the N_2 stream. The resulted protein film was dissolved in 6 M guanidine chloride at 4 °C. Next, 6 M guanidine chloride was replaced with 20 mM phosphate buffer, pH 7.4 using a PD-10 desalting column (Cytiva, Cat. No 17085101; Marlborough, MA, USA). Buffer exchange was performed at 4 °C to suppress peptide aggregation. Final samples contained 60 μM of $A\beta_{1\text{-}42}$ and 240 μM of LUVs; the samples were incubated at 25 °C under quiescent conditions.

Kinetic measurements

Protein aggregation was monitored using a thioflavin T (ThT) fluorescence assay. For this, samples were mixed with ThT at a final concentration of 25 μM. Measurements were performed in 96 wells plate under a quiescent condition at 25 °C using a Multimode microplate reader Tecan Spark, with excitation of 450 nm; the emission signal was collected at 495 nm. Measurements were performed every 5 min. *T*-test was used to determine significance level of t_{lag}, $t_{1/2}$, and t_{grow}.

AFM and AFM-IR

Solutions of protein aggregates were exposed to silicon wafers for 3 min. Next, the excess of the solution has removed; samples were rinsed with DI water and dried at room temperature. AFM and AFM-IR imaging were conducted using a Nano-IR3 system (Bruker, Billerica, MA, USA) equipped with a QCL laser. Contact-mode AFM tips (ContGB-G AFM probe, NanoAndMore, Watsonville, CA, USA) were used to obtain all images, spectra and IR maps. It should be noted that the sample background had no IR signal (Fig. 11). All raw spectra were treated by 10 points smoothing filter in Analysis Studio v3.15 and

normalized by average area. Spectral fitting was performed in GRAMS/AI 7.0 (Thermo Galactic, Salem, NH, USA). Amide I region (1600–1700 cm^{-1}) was fitted with 3 or 4 peaks centered at 1616 and 1636 cm^{-1} (parallel β-sheet), 1667 cm^{-1} (unordered protein) and 1694 cm^{-1} (anti-parallel β-sheet). Peak area for each secondary structure was normalized relative to the total peak area of the amide I region. Corresponding percentages of the amide I band region for each secondary structure were reported in this study. We also performed ANOVA and Tukey's HSD *post hoc t*-test on all spectral classes discussed in this work. Results of ANOVA and Tukey's HSD *post hoc t*-test are summarized in Tables S1, S2 and S4.

Circular dichroism (CD)

CD spectra were collected from all samples at 25 °C using a J-1000 CD spectrometer (Jasco, Easton, MD, USA). For each sample, three spectra were collected within 205–250 nm.

Attenuated total reflectance Fourier-transform infrared (ATR-FTIR) spectroscopy

Sample aliquots were placed onto ATR crystal and dried at room temperature. Spectra were measured using Spectrum 100 FTIR spectrometer (PerkinElmer, Waltham, MA, USA). Three spectra were collected from each sample.

Cell toxicity assays

Mice midbrain N27 cells were grown in RPMI 1640 Medium (Thermo Fisher Scientific, Waltham, MA, USA) with 10% fetal bovine serum (FBS) (Invitrogen, Waltham, MA, USA) in 96 well-plate (5000 cells per well) at 37 °C under 5% CO_2. After 24 h, the cells were found to fully adhere to the wells reaching ~ 70% confluency. Next, 100 μL of the cell culture was replaced with 100 μL RPMI 1640 Medium with 5% FBS containing protein samples. Concentration of FBS was decreased to lower the baseline absorbance level of the control, as required by the LDH assay. After 48 h of incubation, a lactate dehydrogenase (LDH) assay was performed on the cell medium using CytoTox 96 non-radioactive cytotoxicity assay (G1781, Promega, Madison, WI, USA). LDH is a cytosolic enzyme that is released into the surrounding cell culture medium upon damage of the plasma membrane. Concentration of LDH can be quantified by measurement of the conversion of lactate to pyruvate via NAD^+ reduction to NADH, which in turn is used to reduce a tetrazolium salt into a red formazan product that can be measured at 490 nm. Consequently, the level of formazan is directly proportional to the amount of LDH, which, in turns, represents toxicity of certain type of protein aggregates to N27 cells. In our experiments, absorption measurements were made in a plate reader (Tecan, Männedorf, Switzerland) at 490 nm. Every well was measured 25 times in different locations. All measurements were done in triplicates. We performed ANOVA and Tukey's HSD *post hoc t*-test on all classes of samples. Results of ANOVA and Tukey's HSD *post hoc* t-test are summarized in Table S3.

Acknowledgement

We are grateful to the National Institute of Health for the provided financial support (R35GM142869).

Conflict of interest

The authors declare no conflict of interest.

Author contributions

Conceptualization: KZ and DK; Methodology: KZ and DK; Validation: KZ; Data analysis: KZ; Investigation: KZ; Resources: DK; Writing and editing: KZ and DK.

Peer review

The peer review history for this article is available at https://publons.com/publon/10.1111/febs.16738.

Data availability statement

All data described in this manuscript are contained within the manuscript.

References

1 Holtzman DM, Morris JC & Goate AM (2011) Alzheimer's disease: the challenge of the second century. *Sci Transl Med* **3**, 77sr1.
2 Breijyeh Z & Karaman R (2020) Comprehensive review on Alzheimer's disease: causes and treatment. *Molecules* **25**, 5789.
3 Knopman DS, Amieva H, Petersen RC, Chetelat G, Holtzman DM, Hyman BT, Nixon RA & Jones DT (2021) Alzheimer disease. *Nat Rev Dis Primers* **7**, 33.
4 (2021) 2021 Alzheimer's disease facts and figures. *Alzheimers Dement* **17**, 327–406.
5 Long JM & Holtzman DM (2019) Alzheimer disease: an update on pathobiology and treatment strategies. *Cell* **179**, 312–339.
6 Chiti F & Dobson CM (2017) Protein misfolding, amyloid formation, and human disease: a summary of Progress over the last decade. *Annu Rev Biochem* **86**, 27–68.
7 Wesén E, Jeffries GDM, Dzebo MM & Esbjörner EK (2017) Endocytic uptake of monomeric amyloid-β

peptides is clathrin- and dynamin-independent and results in selective accumulation of Aβ(1–42) compared to Aβ(1–40). *Sci Rep* **7**, 2021.
8 Kollmer M, Close W, Funk L, Rasmussen J, Bsoul A, Schierhorn A, Schmidt M, Sigurdson CJ, Jucker M & Fändrich M (2019) Cryo-EM structure and polymorphism of Abeta amyloid fibrils purified from Alzheimer's brain tissue. *Nat Commun* **10**, 4760.
9 Gremer L, Schölzel D, Schenk C, Reinartz E, Labahn J, Ravelli RBG, Tusche M, Lopez-Iglesias C, Hoyer W, Heise H *et al.* (2017) Fibril structure of amyloid-beta(1-42) by cryo-electron microscopy. *Science* **358**, 116–119.
10 Paravastu AK, Qahwash I, Leapman RD, Meredith SC & Tycko R (2009) Seeded growth of beta-amyloid fibrils from Alzheimer's brain-derived fibrils produces a distinct fibril structure. *Proc Natl Acad Sci USA* **106**, 7443–7448.
11 Tycko R (2011) Solid-state NMR studies of amyloid fibril structure. *Annu Rev Phys Chem* **62**, 279–299.
12 Ghosh U, Thurber KR, Yau WM & Tycko R (2021) Molecular structure of a prevalent amyloid-beta fibril polymorph from Alzheimer's disease brain tissue. *Proc Natl Acad Sci USA* **118**, e2023089118.
13 Ghosh U, Yau WM, Collinge J & Tycko R (2021) Structural differences in amyloid-beta fibrils from brains of nondemented elderly individuals and Alzheimer's disease patients. *Proc Natl Acad Sci USA* **118**, e2023089118.
14 Lee M, Ghosh U, Thurber KR, Kato M & Tycko R (2020) Molecular structure and interactions within amyloid-like fibrils formed by a low-complexity protein sequence from FUS. *Nat Commun* **11**, 5735.
15 Kurouski D, Dukor RK, Lu X, Nafie LA & Lednev IK (2012) Normal and reversed supramolecular chirality of insulin fibrils probed by vibrational circular dichroism at the protofilament level of fibril structure. *Biophys J* **103**, 522–531.
16 Kurouski D, Dukor RK, Lu X, Nafie LA & Lednev IK (2012) Spontaneous inter-conversion of insulin fibril chirality. *Chem Commun* **48**, 2837–2839.
17 Kurouski D, Lombardi RA, Dukor RK, Lednev IK & Nafie LA (2010) Direct observation and pH control of reversed supramolecular chirality in insulin fibrils by vibrational circular dichroism. *Chem Commun* **46**, 7154–7156.
18 Sandberg A, Luheshi LM, Söllvander S, Pereira de Barros T, Macao B, Knowles TPJ, Biverstål H, Lendel C, Ekholm-Petterson F, Dubnovitsky A *et al.* (2010) Stabilization of neurotoxic Alzheimer amyloid-beta oligomers by protein engineering. *Proc Natl Acad Sci USA* **107**, 15595–15600.
19 Vosough F & Barth A (2021) Characterization of homogeneous and heterogeneous amyloid-beta42 oligomer preparations with biochemical methods and infrared spectroscopy reveals a correlation between infrared Spectrum and oligomer size. *ACS Chem Nerosci* **12**, 473–488.
20 De Simone A, Naldi M, Tedesco D, Milelli A, Bartolini M, Davani L, Widera D, Dallas ML & Andrisano V (2019) Investigating in vitro amyloid peptide 1-42 aggregation: impact of higher molecular weight stable adducts. *ACS Omega* **4**, 12308–12318.
21 Lipiec E, Perez-Guaita D, Kaderli J, Wood BR & Zenobi R (2018) Direct Nanospectroscopic verification of the amyloid aggregation pathway. *Angew Chem Int ed Engl* **57**, 8519–8524.
22 Krasnoslobodtsev AV, Deckert-Gaudig T, Zhang Y, Deckert V & Lyubchenko YL (2016) Polymorphism of amyloid fibrils formed by a peptide from the yeast prion protein Sup35: AFM and tip-enhanced Raman scattering studies. *Ultramicroscopy* **165**, 26–33.
23 Ramer G, Ruggeri FS, Levin A, Knowles TPJ & Centrone A (2018) Determination of polypeptide conformation with nanoscale resolution in water. *ACS Nano* **12**, 6612–6619.
24 Ruggeri FS, Benedetti F, Knowles TPJ, Lashuel HA, Sekatskii S & Dietler G (2018) Identification and nanomechanical characterization of the fundamental single-strand protofilaments of amyloid alpha-synuclein fibrils. *Proc Natl Acad Sci USA* **115**, 7230–7235.
25 Ruggeri FS, Mannini B, Schmid R, Vendruscolo M & Knowles TPJ (2020) Single molecule secondary structure determination of proteins through infrared absorption nanospectroscopy. *Nat Commun* **11**, 2945.
26 Kurouski D, Deckert-Gaudig T, Deckert V & Lednev IK (2014) Surface characterization of insulin protofilaments and fibril polymorphs using tip-enhanced Raman spectroscopy (TERS). *Biophys J* **106**, 263–271.
27 Ruggeri FS, Vieweg S, Cendrowska U, Longo G, Chiki A, Lashuel HA & Dietler G (2016) Nanoscale studies link amyloid maturity with polyglutamine diseases onset. *Sci Rep* **6**, 31155.
28 Sonntag MD, Klingsporn JM, Garibay LK, Roberts JM, Dieringer JA, Seideman T, Scheidt KA, Jensen L, Schatz GC & van Duyne RP (2012) Single molecule tip enhanced Raman spectroscopy. *J Phys Chem C* **116**, 478–483.
29 Kurouski D, Dazzi A, Zenobi R & Centrone A (2020) Infrared and Raman chemical imaging and spectroscopy at the nanoscale. *Chem Soc Rev* **49**, 3315–3347.
30 Dazzi A & Prater CB (2017) AFM-IR: technology and applications in nanoscale infrared spectroscopy and chemical imaging. *Chem Rev* **117**, 5146–5173.
31 Centrone A (2015) Infrared imaging and spectroscopy beyond the diffraction limit. *Annu Rev Anal Chem* **8**, 101–126.
32 Chae J, An S, Ramer G, Stavila V, Holland G, Yoon Y, Talin AA, Allendorf M, Aksyuk VA & Centrone A (2017) Nanophotonic atomic force microscope

transducers enable chemical composition and thermal conductivity measurements at the nanoscale. *Nano Lett* **17**, 5587–5594.
33 Ramer G, Aksyuk VA & Centrone A (2017) Quantitative chemical analysis at the nanoscale using the photothermal induced resonance technique. *Anal Chem* **89**, 13524–13531.
34 Zhou L & Kurouski D (2020) Structural characterization of individual alpha-synuclein oligomers formed at different stages of protein aggregation by atomic force microscopy-infrared spectroscopy. *Anal Chem* **92**, 6806–6810.
35 Herzberg M, Szunyogh D, Thulstrup PW, Hassenkam T & Hemmingsen L (2020) Probing the secondary structure of individual Abeta40 amorphous aggregates and fibrils by AFM-IR spectroscopy. *Chembiochem* **21**, 3521–3524.
36 Banerjee S & Ghosh A (2021) Structurally distinct polymorphs of tau aggregates revealed by nanoscale infrared spectroscopy. *J Phys Chem Lett* **12**, 11035–11041.
37 Peralvarez-Marin A, Barth A & Graslund A (2008) Time-resolved infrared spectroscopy of pH-induced aggregation of the Alzheimer Abeta(1-28) peptide. *J Mol Biol* **379**, 589–596.
38 Cerf E, Sarroukh R, Tamamizu-Kato S, Breydo L, Derclaye S, Dufrêne YF, Narayanaswami V, Goormaghtigh E, Ruysschaert JM & Raussens V (2009) Antiparallel beta-sheet: a signature structure of the oligomeric amyloid beta-peptide. *Biochem J* **421**, 415–423.
39 Sarroukh R, Goormaghtigh E, Ruysschaert JM & Raussens V (2013) ATR-FTIR: a "rejuvenated" tool to investigate amyloid proteins. *Biochim Biophys Acta* **1828**, 2328–2338.
40 Lomont JP, Rich KL, Maj M, Ho JJ, Ostrander JS & Zanni MT (2018) Spectroscopic signature for stable beta-amyloid fibrils versus beta-sheet-Rich oligomers. *J Phys Chem B* **122**, 144–153.
41 Petty SA & Decatur SM (2005) Experimental evidence for the reorganization of beta-strands within aggregates of the Abeta(16-22) peptide. *J Am Chem Soc* **127**, 13488–13489.
42 Petty SA & Decatur SM (2005) Intersheet rearrangement of polypeptides during nucleation of {beta}-sheet aggregates. *Proc Natl Acad Sci U S A* **102**, 14272–14277.
43 Popova LA, Kodali R, Wetzel R & Lednev IK (2010) Structural variations in the cross-beta core of amyloid beta fibrils revealed by deep UV resonance Raman spectroscopy. *J Am Chem Soc* **132**, 6324–6328.
44 Tempra C, Scollo F, Pannuzzo M, Lolicato F & La Rosa C (2022) A unifying framework for amyloid-mediated membrane damage: the lipid-chaperone hypothesis. *Biochim Biophys Acta Proteins Proteom* **1870**, 140767.
45 Viennet T, Wördehoff MM, Uluca B, Poojari C, Shaykhalishahi H, Willbold D, Strodel B, Heise H, Buell AK, Hoyer W *et al.* (2018) Structural insights from lipid-bilayer nanodiscs link alpha-synuclein membrane-binding modes to amyloid fibril formation. *Commun Biol* **1**, 44.
46 Dou T, Zhou L & Kurouski D (2021) Unravelling the structural Organization of Individual alpha-synuclein oligomers grown in the presence of phospholipids. *J Phys Chem Lett* **12**, 4407–4414.
47 Rizevsky S, Matveyenka M & Kurouski D (2022) Nanoscale structural analysis of a lipid-driven aggregation of insulin. *J Phys Chem Lett* **13**, 2467–2473.
48 Zhang X, St Clair JR, London E & Raleigh DP (2017) Islet amyloid polypeptide membrane interactions: effects of membrane composition. *Biochemistry* **56**, 376–390.
49 Rice AC, Ladd AC & Bennett JP Jr (2015) Postmortem Alzheimer's disease hippocampi show oxidative phosphorylation gene expression opposite that of isolated pyramidal neurons. *J Alzheimers Dis* **45**, 1051–1059.
50 Letellier T, Heinrich R, Malgat M & Mazat JP (1994) The kinetic basis of threshold effects observed in mitochondrial diseases: a systemic approach. *Biochem J* **302** (Pt 1), 171–174.
51 Barrientos A & Moraes CT (1999) Titrating the effects of mitochondrial complex I impairment in the cell physiology. *J Biol Chem* **274**, 16188–16197.
52 Iijima-Ando K, Hearn SA, Shenton C, Gatt A, Zhao L & Iijima K (2009) Mitochondrial mislocalization underlies Abeta42-induced neuronal dysfunction in a drosophila model of Alzheimer's disease. *PLoS One* **4**, e8310.
53 Trushina E, Nemutlu E, Zhang S, Christensen T, Camp J, Mesa J, Siddiqui A, Tamura Y, Sesaki H, Wengenack TM *et al.* (2012) Defects in mitochondrial dynamics and metabolomic signatures of evolving energetic stress in mouse models of familial Alzheimer's disease. *PLoS One* **7**, e32737.
54 Qin W, Haroutunian V, Katsel P, Cardozo CP, Ho L, Buxbaum JD & Pasinetti GM (2009) PGC-1alpha expression decreases in the Alzheimer disease brain as a function of dementia. *Arch Neurol* **66**, 352–361.
55 Wang W, Zhao F, Ma X, Perry G & Zhu X (2020) Mitochondria dysfunction in the pathogenesis of Alzheimer's disease: recent advances. *Mol Neurodegener* **15**, 30.
56 Stace CL & Ktistakis NT (2006) Phosphatidic acid- and phosphatidylserine-binding proteins. *Biochim Biophys Acta* **1761**, 913–926.
57 Pope S, Land JM & Heales SJ (2008) Oxidative stress and mitochondrial dysfunction in neurodegeneration; cardiolipin a critical target? *Biochim Biophys Acta* **1777**, 794–799.

58 Falabella M, Vernon HJ, Hanna MG, Claypool SM & Pitceathly RDS (2021) Cardiolipin, mitochondria, and neurological disease. *Trends Endocrinol Metab* **32**, 224–237.
59 Fitzner D, Bader JM, Penkert H, Bergner CG, Su M, Weil MT, Surma MA, Mann M, Klose C & Simons M (2020) Cell-type- and brain-region-resolved mouse brain lipidome. *Cell Rep* **32**, 108132.
60 Michaelson DM, Barkai G & Barenholz Y (1983) Asymmetry of lipid organization in cholinergic synaptic vesicle membranes. *Biochem J* **211**, 155–162.
61 Matveyenka M, Rizevsky S & Kurouski D (2022) Unsaturation in the fatty acids of phospholipids drastically alters the structure and toxicity of insulin aggregates grown in their presence. *J Phys Chem Lett* **13**, 4563–4569.
62 Rizevsky S, Zhaliazka M, Dou T & Matveyenka M (2022) Characterization of substrates and surface-enhancement in atomic force microscopy infrared (AFM-IR) analysis of amyloid aggregates. *J Phys Chem C* **126**, 4157–4162.
63 Coles M, Bicknell W, Watson AA, Fairlie DP & Craik DJ (1998) Solution structure of amyloid beta-peptide(1-40) in a water-micelle environment. Is the membrane-spanning domain where we think it is? *Biochemistry* **37**, 11064–11077.
64 Bera S, Korshavn KJ, Kar RK, Lim MH, Ramamoorthy A & Bhunia A (2016) Biophysical insights into the membrane interaction of the core amyloid-forming Abeta40 fragment K16-K28 and its role in the pathogenesis of Alzheimer's disease. *Phys Chem Chem Phys* **18**, 16890–16901.
65 Kochan K, Perez-Guaita D, Pissang J, Jiang JH, Peleg AY, McNaughton D, Heraud P & Wood BR (2018) In vivo atomic force microscopy-infrared spectroscopy of bacteria. *J Royal Soc Interface* **15**, 20180115.
66 Williams TL, Johnson BR, Urbanc B, Jenkins AT, Connell SD & Serpell LC (2011) Abeta42 oligomers, but not fibrils, simultaneously bind to and cause damage to ganglioside-containing lipid membranes. *Biochem J* **439**, 67–77.
67 Williams TL & Serpell LC (2011) Membrane and surface interactions of Alzheimer's Abeta peptide--insights into the mechanism of cytotoxicity. *FEBS J* **278**, 3905–3917.
68 Ege C & Lee KY (2004) Insertion of Alzheimer's a beta 40 peptide into lipid monolayers. *Biophys J* **87**, 1732–1740.
69 Chi EY, Ege C, Winans A, Majewski J, Wu G, Kjaer K & Lee KY (2008) Lipid membrane templates the ordering and induces the fibrillogenesis of Alzheimer's disease amyloid-beta peptide. *Proteins* **72**, 1–24.
70 Arispe N, Pollard HB & Rojas E (1996) Zn^{2+} interaction with Alzheimer amyloid beta protein calcium channels. *Proc Natl Acad Sci USA* **93**, 1710–1715.
71 Lin H, Bhatia R & Lal R (2001) Amyloid beta protein forms ion channels: implications for Alzheimer's disease pathophysiology. *FASEB J* **15**, 2433–2444.
72 Zhaliazka K & Kurouski D (2022) Nanoscale characterization of parallel and antiparallel beta-sheet amyloid Beta 1-42 aggregates. *ACS Chem Nerosci* **13**, 2813–2820.
73 Cataldi R, Chia S, Pisani K, Ruggeri FS, Xu CK, Šneideris T, Perni M, Sarwat S, Joshi P, Kumita JR *et al.* (2021) A dopamine metabolite stabilizes neurotoxic amyloid-beta oligomers. *Commun Biol* **4**, 19.
74 Jan A, Adolfsson O, Allaman I, Buccarello AL, Magistretti PJ, Pfeifer A, Muhs A & Lashuel HA (2011) Abeta42 neurotoxicity is mediated by ongoing nucleated polymerization process rather than by discrete Abeta42 species. *J Biol Chem* **286**, 8585–8596.
75 Chauhan A, Ray I & Chauhan VP (2000) Interaction of amyloid beta-protein with anionic phospholipids: possible involvement of Lys28 and C-terminus aliphatic amino acids. *Neurochem Res* **25**, 423–429.
76 Matveyenka M, Zhaliazka K, Rizevsky S & Kurouski D (2022) Lipids uniquely alter secondary structure and toxicity of lysozyme aggregates. *FASEB J* **36**, e22543.
77 Matveyenka M, Rizevsky S & Kurouski D (2022) Amyloid aggregates exert cell toxicity causing irreversible damages in the endoplasmic reticulum. *Biochim Biophys Acta Mol Basis Dis* **1868**, 166485.
78 Matveyenka M, Rizevsky S, Pellois JP & Kurouski D (1868) Lipids uniquely alter rates of insulin aggregation and lower toxicity of amyloid aggregates. *Biochim Biophys Acta Mol Cell Biol Lipids* **2023**, 159247.
79 Matveyenka M, Rizevsky S & Kurouski D (2022) The degree of unsaturation of fatty acids in phosphatidylserine alters the rate of insulin aggregation and the structure and toxicity of amyloid aggregates. *FEBS Lett* **596**, 1424–1433.
80 Matveyenka M, Rizevsky S & Kurouski D (2022) Length and unsaturation of fatty acids of phosphatidic acid determines the aggregation rate of insulin and modifies the structure and toxicity of insulin aggregates. *ACS Chem Nerosci* **13**, 2483–2489.

Supporting information

Additional supporting information may be found online in the Supporting Information section at the end of the article.

Table S1. One-way ANOVA of significant differences for all testing groups. Tukey's HSD *post hoc* was performed for multiple comparison procedures, and the statistical test showed the following difference between tested groups.

Table S2. One-way ANOVA of significant differences for all testing groups of Aβ fibrils. Tukey's HSD *post hoc* was performed for multiple comparison procedures, and the statistical test showed the following difference between tested groups.

Table S3. One-way ANOVA of significant differences for all testing groups of samples accordingly to LDH test. Tukey's HSD *post hoc* was performed for multiple comparison procedures, and the statistical test showed the following difference between tested groups.

Table S4. One-way ANOVA of significant differences for all testing groups of Aβ oligomers. Tukey's HSD *post hoc* was performed for multiple comparison procedures, and the statistical test showed the following difference between tested groups.